UWB Microwave Functional Brain Activity Extraction for Parkinson's Disease Monitoring

Youness Akazzim, César Palacios Arias, *Member, IEEE*, Marc Jofre, Otman EL Mrabet, *Member, IEEE*, Jordi Romeu, *Fellow, IEEE*, and Luis Jofre-Roca, *Life Fellow, IEEE*

***Abstract*—Microwaves have proven their imaging capabilities to visualize the body composition for medical applications, thanks to their penetration inside biological structures. In this context, this article presents a novel methodology that aims to extract not just the internal morphology, but also the brain's functional activity using the UWB pulse amplitude modulation (PAM) technique to have simultaneously functional monitoring and imaging capability and apply it to monitor the Parkinson's disease (PD). The radio-frequency system is composed of two orthogonal sets of double UWB probes operating in the frequency range of 0.5–1.5 GHz. An experimental setup has been devised that avoids complex in vivo testing, albeit allows a system proof-of-concept validation. A bio-tag (BT) consisting of an optically modulated photodiode is used to emulate local medium changes associated with cell activity. The proposed system is used to first extract the modeled brain action potential (AP) to validate the performance of the BT and then to monitor the PD based on the beta frequency band character within basal ganglia–thalamocortical (BGTC) which is a key marker for the PD. The results show a good capability of locating and differentiating the signals generated within the phantom by the BT, alternatively emulating the healthy and PD's state, based on the frequency. The obtained results of the functional monitoring technique on distinguishing the healthy from nonhealthy brain model activity, as well as in the phantom mimicking the average proprieties of a human head, will serve as a basis for detecting functional diseases in the future.**

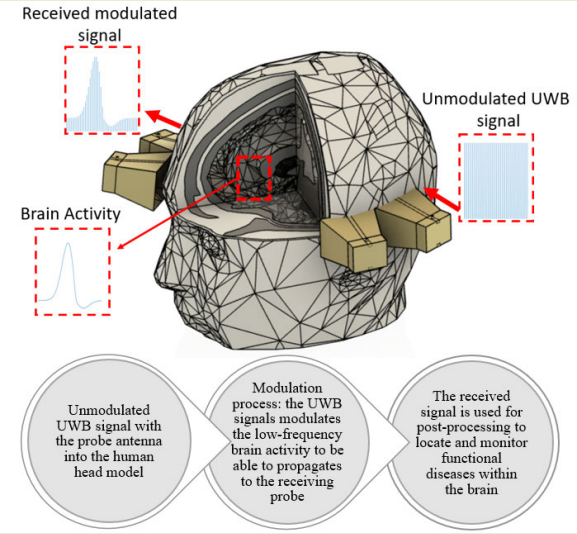

***Index Terms*— Action potential (AP), functional diseases, Parkinson's disease (PD), UWB functional imaging, UWB pulse amplitude modulation (PAM).**

Manuscript received 21 November 2023; accepted 6 December 2023. Date of publication 15 December 2023; date of current version 31 January 2024. This work was supported in part by Comision Interministerial de Ciencia y Tecnologia (CICYT) PID2019-107885GB-C31, PID2022-136869NB-C31, Catalan Research Group 2021 SGR 01415, Metropolis PLEC2021-007609, (FI-SDUR) under Grant 2021 FISDU 00195; in part by the PDR-2014-2022/56-30157-2021-2A grant of the Generalitat de Catalunya; and in part by the Prueba de Concepto PDC2022-133091-I00 grants of the Ministerio de Ciencia, Innovación y Universidades (Spain). The associate editor coordinating the review of this article and approving it for publication was Prof. Huang Chen Lee. *(Corresponding author: Youness Akazzim.)*

Youness Akazzim is with the Department of Signal Theory and Communications, Technical University of Catalonia, Barcelona 08034, Spain, and also with the Intelligent Systems Design Laboratory (ISDL), FS, Abdelmalek Essaadi University, Tetouan 93002, Morocco (e-mail: youness.akazzim@upc.edu).

César Palacios Arias, Jordi Romeu, and Luis Jofre-Roca are with the Department of Signal Theory and Communications, Technical University of Catalonia, Barcelona 08034, Spain.

Marc Jofre is with the Department of Network Engineering, Technical University of Catalonia, Barcelona 08034, Spain.

Otman EL Mrabet is with the Intelligent Systems Design Laboratory (ISDL), FS, Abdelmalek Essaadi University, Tetouan 93002, Morocco.

Digital Object Identifier 10.1109/JSEN.2023.3341168

I. Introduction

THE use of microwaves in medical applications is a promising solution for human body monitoring, thanks to its advantages in terms of innocuity, portability, and cost. Based on the difference in electrical properties of the internal composition of the human body tissues, numerous studies have been conducted for microwave imaging [1], [2], [3], [4], [5], [6], [7], sensing [8], [9], [10], or functional signal extraction of the brain or the heart [11], [12], [13], [14] using single-frequency analysis.

Due to the progressive death of neurons with age, neurodegenerative or functional pathologies such as Parkinson's disease (PD) or Alzheimer's disease (AD) [15], [16] have become one of the most spread illnesses. The World Health Organization (WHO) reports that PD has doubled in the last 25 years, and the global estimates show over 8.5 million individuals with PD (with an increase of 81% since 2000) and caused 329 000 deaths [17].

The main cause of PD is the loss of dopamine in the midbrain substantia nigra [18], which leads to a progressive

neurodegenerative disorder. The PD symptoms start appearing after the loss of more than 60% of the dopaminergic neurons or 80% of dopamine concentration in the putamen [19], [20], [21]. There are treatments available for PD based on medicines such as Levodopa that provides the brain with dopamine [22], or surgical as deep brain stimulation (DBS) [23], [24], but just applied in advanced stages of the illness.

Diagnostic methods for neurodegenerative diseases, some of them initially intended for cancer detection, are functional magnetic resonance imaging (fMRI), computed tomography scans (CT scans), or positron emission tomography scans (PET scans). These techniques have drawbacks such as patients must undergo numerous tests and scans; additionally, these approaches may be expensive, uncomfortable, or inconclusive.

For the early-stage diagnosis and monitoring of PD, researchers explore specific markers that help in understanding the progression of the disease for early treatment. These markers can be clinical as tremors [25], biochemical as neural density [26], prodromal as rapid eye movement (REM) [27], pathophysiological as the loss of the dopaminergic neurons which decreases gradually in the substancia nigra [28] and affects the firing rate of the action potential (AP) [29], or the changes in the beta frequency band oscillatory character that happens in the basal ganglia–thalamocortical (BGTC) [14], [30], [31], [32]. The functional signal extraction within the brain has been studied for different contact–electrode applications using a single-frequency technique as for the brain rat [11], the human brain [13], and recently in the basal ganglia to monitor PD [14], but clearly different for the extraction of the brain activity in terms of both the wireless contact-less character and the focusing capability of the microwave technique proposed in this work.

In this article, we propose a novel method that combines locating the origin of the signal related to the functional disease using UWB imaging and extracting these specific electrical activities using the UWB pulse amplitude modulation (PAM) [33], [34] to differentiate the healthy from the parkinsonism brain based on the beta frequency band oscillatory character. The radiating system is composed of four extended gap ridge horn (EGRH) antennas [1], distributed in two orthogonal sets of double UWB probes. A low RF disturbing bio-tag (BT) element, based on a GHz operation response photodiode, is first used to insert a millisecond time-varying signal, to validate the system capability by extracting the brain spikes up to kHz frequencies [35], [36] within a medium mimicking the human head permittivity. This BT is then used as the origin of the frequency band oscillatory within basal ganglia to produce the frequency signal of 20 Hz to mimic the healthy brain and 15 Hz for the parkinsonism one [14].

The remainder of this article is organized as follows. Section II presents the proposed functional imaging system, as well as the circuital and electromagnetic analysis of the BT used to generate the functional signals. In Section III, the numerical and experimental validation is conducted to prove the capability of the system to detect a functional activity such as the AP within the human head–brain model. In Section IV, an experimental analysis of the beta frequency band oscillation changes for differentiating between two signals representing the healthy and PD's state based on the firing rate frequency is discussed. Finally, preliminary conclusions are presented in Section V.

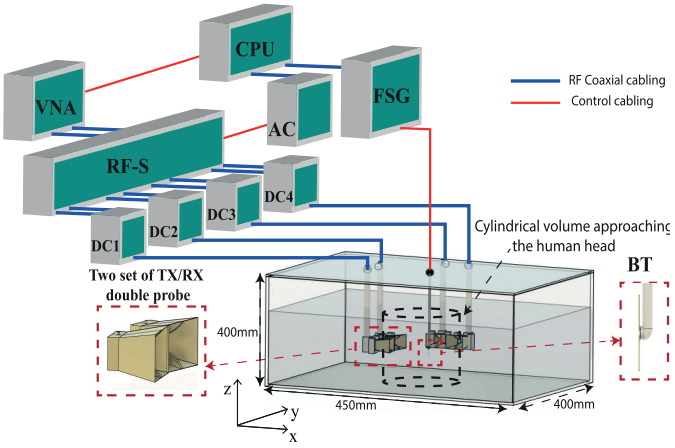

Fig. 1. Functional monitoring system, where the transmitting and receiving RF links are selected by the ac to measure the functional changes of the BT within the tank of liquid mimicking the human head–brain medium.

II. Functional Microwave System

In this section, the setup used to validate the proposed method for microwave functional diseases is presented in Fig. 1, which consists of two main subsystems.

1) The UWB imaging system: containing an orthogonal set of two EGRH probes [1], [37], sequentially connected to a TX/RX vector network analyzer (VNA) collecting the 4×4 UWB scattering parameters.
2) The functional signal modeling unit BT: composed of a photodiode illuminated through an optical fiber by an LED [38] emitting a P_{inc} blue light power.

These two subsystems are connected to a computer controlling the different instruments and processing the measured S-parameters to locate the BT and extract the functional signals.

A. UWB Imaging Subsystem

The UWB imaging system in Fig. 1 contains the RF Tx/Rx addressing circuitry and the four radiating elements (probes). The RF subsystem sequentially addresses (through a combination of two RF switches (RF-S) and four directional couplers (DCi, $i = 1$–4) controlled by an Arduino (UNO) unit) the Tx and Rx ports of the VNA ZNB 40 R&S to each one of the 4 UWB EGRH probes emitting power of $P_{\text{EGRH}} = 10$ dBm to the head model. The system is located inside a liquid tank with overall dimensions of $450 \times 400 \times 400$ mm^3, filled with liquid material mimicking the human head–brain medium of permittivity $\varepsilon_r \simeq 57.0$ and $\sigma \simeq 0.6$ S/m [39], forming an optimized imaging geometry of two 90° separation double-probe sets [1] forming a virtual cylinder in black that has a diameter of $d_{\text{phn}}^{\text{brn}} = 200$ mm approaching the average size of a simplified human head. The RF subsystem is immersed in the liquid and the container to have simultaneously the virtual head model and the matching liquid inside the probe antennas to minimize the reflections from the contour of the phantom.

To protect the photodiode, it is covered with a thin plastic layer that also keeps the optical fiber oriented to the active zone of the photodiode, and it is placed in a position shifted from the equivalent center of the brain which corresponds to the one pair of the substantia nigra [40].

A control processing unit (CPU), is a computer that connects all the hardware parts. It contains a dual-core processor with 64 GB of RAM that processes the results in less than 6 min and sends the necessary commands to the VNA and Arduino Control (ac) units, to collect the set of complex (amplitude and phase) measured scattering signals sending in parallel the necessary commands to the functional signal generator (FSG) to produce the different functional activity signals in the BT.

B. Equivalence of the Photodiode With the Cellular Membrane Behavior

Cellular, as well as intracellular, membranes exhibit a distinct nonlinear electrical behavior due to the potential barrier resulting from the difference between the inner and outer electrolytes and the action of ion pumps [41]. In the absence of an applied electromagnetic field, the transmembrane potential difference $\Delta\phi$ is equal to the cell "resting" potential V_0 ($\simeq -100$ mV for a typical cell) [42]. When a cell enters an active membrane potential state, it generates itself a low-frequency (in the order of up to kHz) transmembrane voltage excess potential $\Delta\phi = V_0 + \delta\phi$ (resulting in $\Delta\phi = 40$ mV). On top of the self-generated low-frequency voltage, the illuminating external microwave signal like the one analyzed in this work (the cell is relatively sensitive to these electromagnetic frequencies) adds a high-frequency small-signal transmembrane voltage excess potential on the cell, which is proportional to the electric field applied. As a result, a transmembrane current density $\vec{J}_m$ (having the two components corresponding to the self-generated low-frequency signal $f_{\text{lf}}^{\text{sg}}$ and to the externally induced microwave signal $f_{\text{mw}}^{\text{ei}}$) is generated. The current–voltage response of the membrane is known to be fairly well approximated by a nonlinear diode-like relationship of the form $\vec{J}_m = J_0(e^{(\delta\phi/V_T)} - 1)$ with typical values in the order of $J_0 \simeq 10^{-5}$ A/cm^2 and $V_T \simeq 5$ mV [43]. As a result of the nonlinear behavior of the cellular membrane, a combined modulated signal will appear carrying the specific information of the membrane state $f_{\text{lf}}^{\text{sg}} \pm f_{\text{mw}}^{\text{ei}}$. For the case of the specific cellular functional activities considered here, the active regions may be approached by a circular surface with diameter in the order of 10 to 50 μm result in the transmembrane current–voltage $(I_m, \delta\phi)$ point value in the order of (0.1 nA, 0 V) for the "rest" and (1 mA, 100 mV) for the "active" states [43], [44]. In this way, when a cell is illuminated at a frequency $f_{\text{mw}}^{\text{ei}}$, we will recover a "structural nonmodulated" signal at the same $f_{\text{mw}}^{\text{ei}}$ frequency corresponding to the volumetric cell scattering and a "transmembrane modulated" signal at the frequency $f_{\text{lf}}^{\text{sg}} \pm f_{\text{mw}}^{\text{ei}}$ corresponding to the scattering produced by the changing membrane. Our interest will focus on recovering this modulated signal because it is the component carrying the information on the membrane's functional state. As elaborated in [44] for a frequency of 1 GHz the ratio between the two field components corresponding to the "membrane-modulated" and the "structural-nonmodulated" will be in the order of -90 dB that will require high-sensitivity (high dynamic range) detection systems. To produce the modulating signals mimicking the brain functional activity as mentioned above (i.e., Parkinson-like signals) the combination of a photodiode FDS015 from Thorlabs [38] with an active area of 10 $\times$ 10 μm^2 and overall size of 20.0 $\times$ 4.7 $\times$ 6.4 mm^3 connected through an optical fiber to an LED modulator M455F3 [45] is used. The unit is fed by a 2000 series picoscope generator able to generate the different signals (the ON PD electric state to simulate the "active biological state" and the OFF PD electrical state to simulate the "resting biological state").

TABLE I
PARAMETERS OF THE PHOTODIODE MODEL

Parameter	Equation (resource)	Value
I_{bt}	Bio-tag current $I_{bt} = P_{inc} \times R_\lambda$ Responsivity of FDS015 $R_\lambda = 0.16\,A/W$ Incident power $P_{inc} = 5\,mW$	0.8 mA
I_D	Dark current from datasheet [38]	0.03 nA
C_J	Junction Capacitance from datasheet [38]	0.65 pF
R_{sh}	Shunt resistance from datasheet [38]	100 kOhm

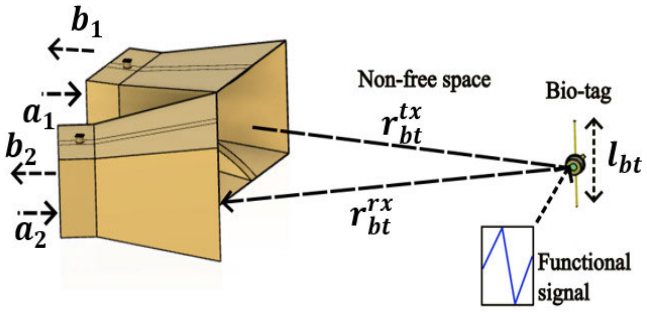

Fig. 2. Modulated backscattered signal scenario.

Based on its equivalent circuit [38] (the parameters in Table I), the ON and OFF values of its corresponding impedance were obtained. The data has been extracted for the center frequency $f_{\text{cn}} = 1$ GHz of the operating frequency band of the EGRH probes 0.5–1.5 GHz. In the case of the photodiode driven with a $I_{\text{bt}} = 0.8$ mA, which corresponds to the maximum incident power $P_{\text{inc}} = 5$ mW, the simulated complex impedance (ON state) is $Z_{L1}^{\text{ON}} \simeq (31.7 - j4.2)\ \Omega$. When the photodiode is OFF (dark current 0.03 nA), the equivalent impedance is $Z_{L2}^{\text{OFF}} \simeq (0.6 - j244.8)\ \Omega$. The values of the current generated at the photodiode for both electrical ON (bio-active state) of 0.8 mA and electrical OFF (bio-rest state) of 0.03 nA approach quite well the currents passing through the cellular membrane mentioned above of 1 mA and 0.1 nA, respectively, that guarantees similar radiated values for the cellular membrane and the photodiode.

C. Electromagnetic Analysis of the BT

As previously mentioned, the BT when illuminated by an incident RF signal (as in Fig. 2) will be responsible for approaching the effect of the cells creating the low-frequency functional signals AP, resulting in the modulating effect

produced by the nonlinear behavior of the cell membrane, and finally reradiating back the RF modulated signal. This BT may be modeled as the combination of a modulating photodiode with impedances Z_{L1}^{ON} and Z_{L2}^{OFF} and a radiating elements formed by its actual leads. In this way, when the BT is illuminated by the RF incident field radiated by the corresponding Tx probe, the induced RF currents into the photodiode produce a modulated reradiated (scattered) signal due to the nonlinear effect of the diode that is significantly below the nonmodulated component due to structural radiation of the photodiode, similar to what it will happen into the real biological cell where the membrane-modulated scattered signal is significantly below the scattering produced by the whole cell.

In the following, the basic electromagnetic expressions of the scattering effect are presented. The photodiode with its leads is first modeled as a dipole of length l_{bt} (20 mm, in the order of a half-wave dipole in the brain medium at the operating band) loaded alternatively with a modulating impedance $(Z_{L1}^{\mathrm{ON}}, Z_{L2}^{\mathrm{OFF}})$.

The equivalent impedance of the photodiode's leads $Z_{\mathrm{bt}}^{\mathrm{hw}}$ is calculated using (1) [46] as follows:

$$Z_{\mathrm{bt}}^{\mathrm{hw}} = \left(73 + j43\frac{l_{\mathrm{bt}}/\lambda_{\mathrm{phn}}^{\mathrm{brn}} - 0.45}{0.05}\right)\Omega \tag{1}$$

where $\lambda_{\mathrm{phn}}^{\mathrm{brn}}$ is the wavelength within the head–brain medium.

The differential scattered field (difference between the modulated and the nonmodulated scattered fields) produced by the BT can be obtained by (2) as in [47] and [48] the following equation:

$$\Delta\sigma_{\mathrm{bt}} = \frac{\left(\lambda_{\mathrm{phn}}^{\mathrm{brn}} G_{\mathrm{bt}}^{\mathrm{hw}}\right)^2}{4\pi}|\rho_{L1} - \rho_{L1}|^2 \tag{2}$$

where $\rho_{L1} = (Z_{L1}^{\mathrm{ON}} - (Z_{\mathrm{bt}}^{\mathrm{hw}})^*/Z_{L1}^{\mathrm{ON}} + Z_{\mathrm{bt}}^{\mathrm{hw}})$, $\rho_{L2} = (Z_{L2}^{\mathrm{OFF}} - (Z_{\mathrm{bt}}^{\mathrm{hw}})^*/Z_{L2}^{\mathrm{OFF}} + Z_{\mathrm{bt}}^{\mathrm{hw}})$, and $G_{\mathrm{bt}}^{\mathrm{hw}}$ is the antenna gain of the photodiode leads modeled as a half-wave dipole.

The modulated part of the backscattered signal from the BT at the receiving probe can be written as follows:

$$\Delta S_{21}^{\mathrm{mod}} = \frac{\left(\lambda_{\mathrm{phn}}^{\mathrm{brn}}\right)^2 G_p^2 \Delta\sigma_{\mathrm{bt}}}{(4\pi)^3 \left(r_{\mathrm{bt}}^{\mathrm{rx}}\right)^4} \exp\left(-2\alpha_{\mathrm{phn}}^{\mathrm{brn}} r_{\mathrm{bt}}^{\mathrm{rx}}\right) \tag{3}$$

where G_p is the gain of the probe antenna and $\alpha_{\mathrm{phn}}^{\mathrm{brn}}$ is the attenuation in the human head–brain medium.

For $l_{\mathrm{bt}} = 20$ mm and $G_{\mathrm{bt}}^{\mathrm{hw}} = 1.64$ dB, $G_p = 8$ dB, $\alpha_{\mathrm{phn}}^{\mathrm{brn}} = 1$ dB/cm, and $r_{\mathrm{bt}}^{\mathrm{rx}} = 100$ mm at $f_{\mathrm{phn}}^{\mathrm{brn}} = 1$ GHz, the differential scattering field is calculated analytically using (3) and results in $\Delta S_{21}^{\mathrm{mod}} \simeq -92$ dB. To detect the variation of equivalent impedance produced by the BT, we need a dynamic range larger than -90 dB (in the order of 120 dB), compatible with the sensitivity levels of the actual network analyzer.

D. Functional Signals Generation

In this section, we validate the BT on producing functional signals within the head–brain medium based on the equivalent impedance change of the photodiode. The interaction process between the brain nerves can be seen as chemical for the neurotransmitters such as the dopamine in the Synaptic Cleft, or equivalently electrical for the AP based on different membrane potential in the axons [49].

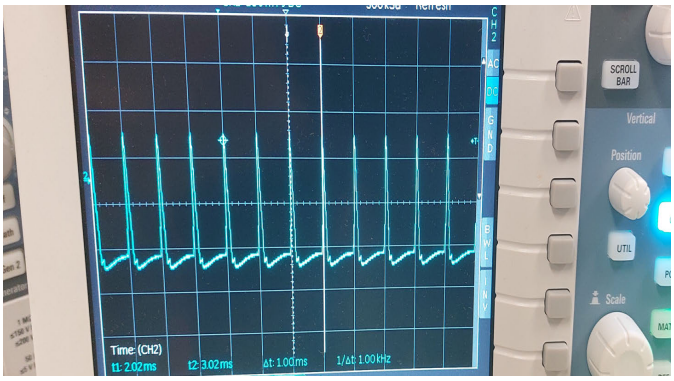

Fig. 3. Experimentally generated AP using the BT.

The experimental operation of the AP has been conducted by illuminating the BT with a blue light LED oriented to the active zone of the photodiode through an optical fiber controlled by the signal generator Picoscope 2000 series, approaching the shape of the AP. The voltage values for the two states of the photodiode measured with the high impedance oscilloscope are $V_{\mathrm{bt}}^{\mathrm{ON}} \simeq 140$ mV when it is ON, and $V_{\mathrm{bt}}^{\mathrm{ON}} \simeq 0.2$ mV when it is OFF, with $\Delta V_{\mathrm{bt}} \simeq 140$ mV, close to the values of the cell membrane. The real-time signal generated by the BT to model the AP is presented in Fig. 3, which has a frequency in the order of $f_{\mathrm{bt}} \simeq 1$ kHz, which mimics the firing rate of a realistic brain AP spike -1 ms duration [50].

III. Numerical and Experimental Validation

This section presents the validation of the proposed functional microwave system, which is the combination of two operations: locating the origin of the targeted functional activity by using the UWB RF signals and extracting the functional activity parameters (firing rate and shape) from the backscattered modulated signals using the pulse amplitude demodulation.

An initial analysis studied the safety of the applied power and the sensitivity to the antenna–head probe distance. For the safety for the applied input power of $P_{\mathrm{EGRH}} = 10$ dBm, the specific absorption rate (SAR) is shown in Fig. 4 for 1 and 10 g of human tissue, where the obtained value at 1 GHz is 0.62 and 0.20 W/kg, respectively, are below the limit (1.60 and 2.00 W/kg). For an antenna–head tissue separation sensitivity, it was seen that changes up to 10 mm do not significantly affect either the dimension or the location of the reconstructed PD region. In Fig. 5, the experimental setup used for the functional monitoring is presented, where the VNA is connected to two PC-controlled RF-S that create the transmitting and receiving links from the VNA's ports to the probe antennas.

The results were extracted during a time range of $T_{\mathrm{max}} = 10$ ms, in which the MATLAB script is used to collect the data from the CST software and the VNA for the numerical and the

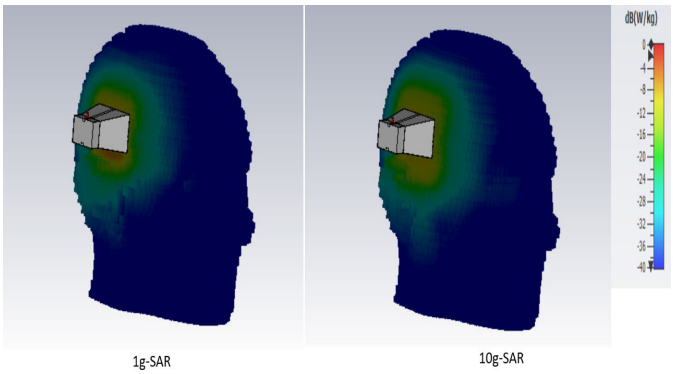

Fig. 4. SAR for the human head model for 1 and 10 g of tissue.

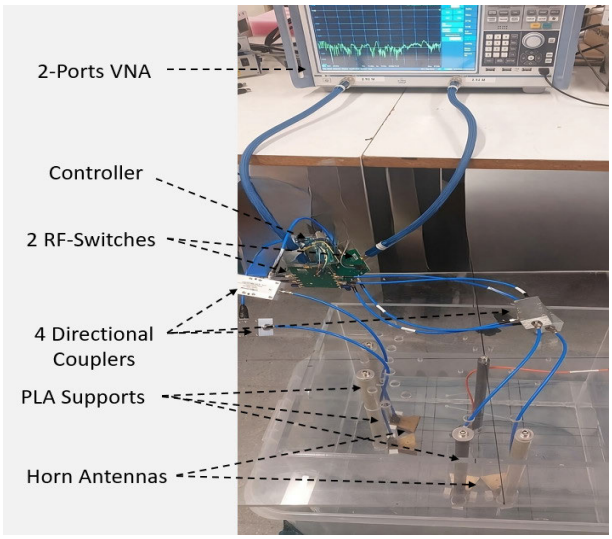

Fig. 5. Experimental hardware diagram.

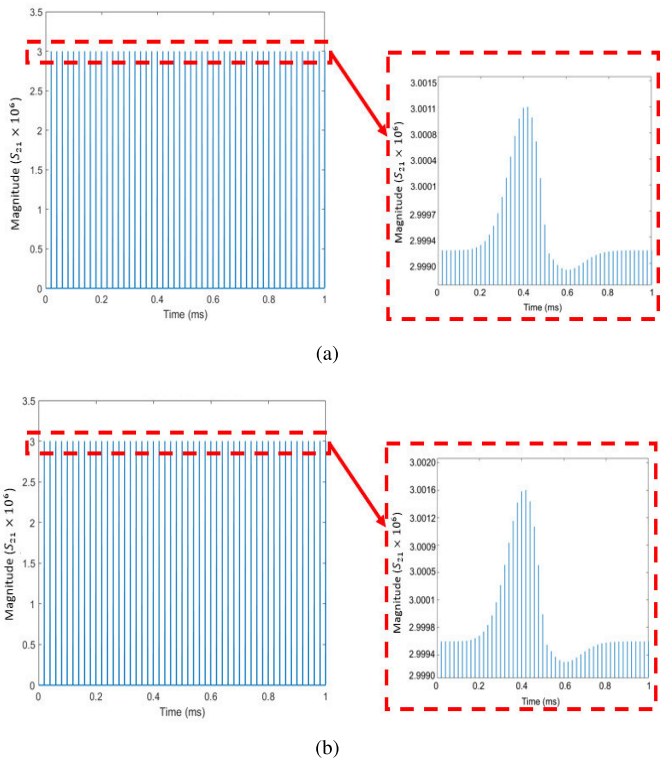

Fig. 6. Backscatter pulse amplitude-modulated signal. (a) Numerical results. (b) Experimental results.

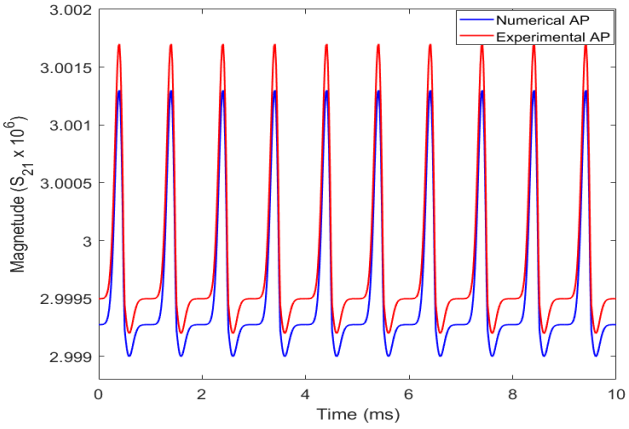

Fig. 7. Numerical and the experimentally extracted AP signal.

experimental validation processes, respectively, as previously mentioned in Fig. 1.

A signal generator is used to create the AP shape on the BT within the small signals' regime, modulating the UWB RF signals transmitted by the probes using the PAM.

The UWB scattering parameters are extracted for 50 samples, with a time step between samples of $\Delta t = 20\ \mu$s. The corresponding measured matrix is transformed to the time domain and delayed by $n \times \Delta t$ (where $n = 1, 2, \ldots 50$), resulting in a PAM received signal, which contains the UWB pulses enveloped by the AP, as presented for 1 ms period of the simulated signal in Fig. 6(a), and in Fig. 6(b) for the measured one, where we can observe the modulation of the UWB pulses with the functional signal modeling the brain activity.

After demodulating the signal for a time extension of 10 ms (ten periods of the signal in Fig. 6), the AP obtained is presented in Fig. 7, where we can identify and compare the functional signal obtained by the BT located within the head–brain model for the simulated and measured setup. An AP firing rate of $f_{bt} = 1$ kHz may be observed in accordance with the modulating signal produced by the active zone of the photodiode, mimicking the real brain spiking.

The subtraction of the scattered parameter measurement for the two ON and OFF states will allow keeping the usefully modulated component and remove the nondesired reflections coming from the measurement environment, resulting in the signal represented in Fig. 7. Then, by applying the Multi-frequency Bifocusing (MFBF) algorithm [51], we reconstruct the microwave image that allows locating the BT (modeling the brain activity within the PD region) as in Fig. 8 for the numerical and experimental results.

In Fig. 8(a), a realistic human head model used for the numerical validation with skin, skull, CSF, grey, and white matter is presented, where the red circle refers to the studied region related to the PD. The BT is used to model the functional signals produced on the right side of the basal ganglia to approach the near-to-reality scenario. The model is validated numerically with CST software using the system

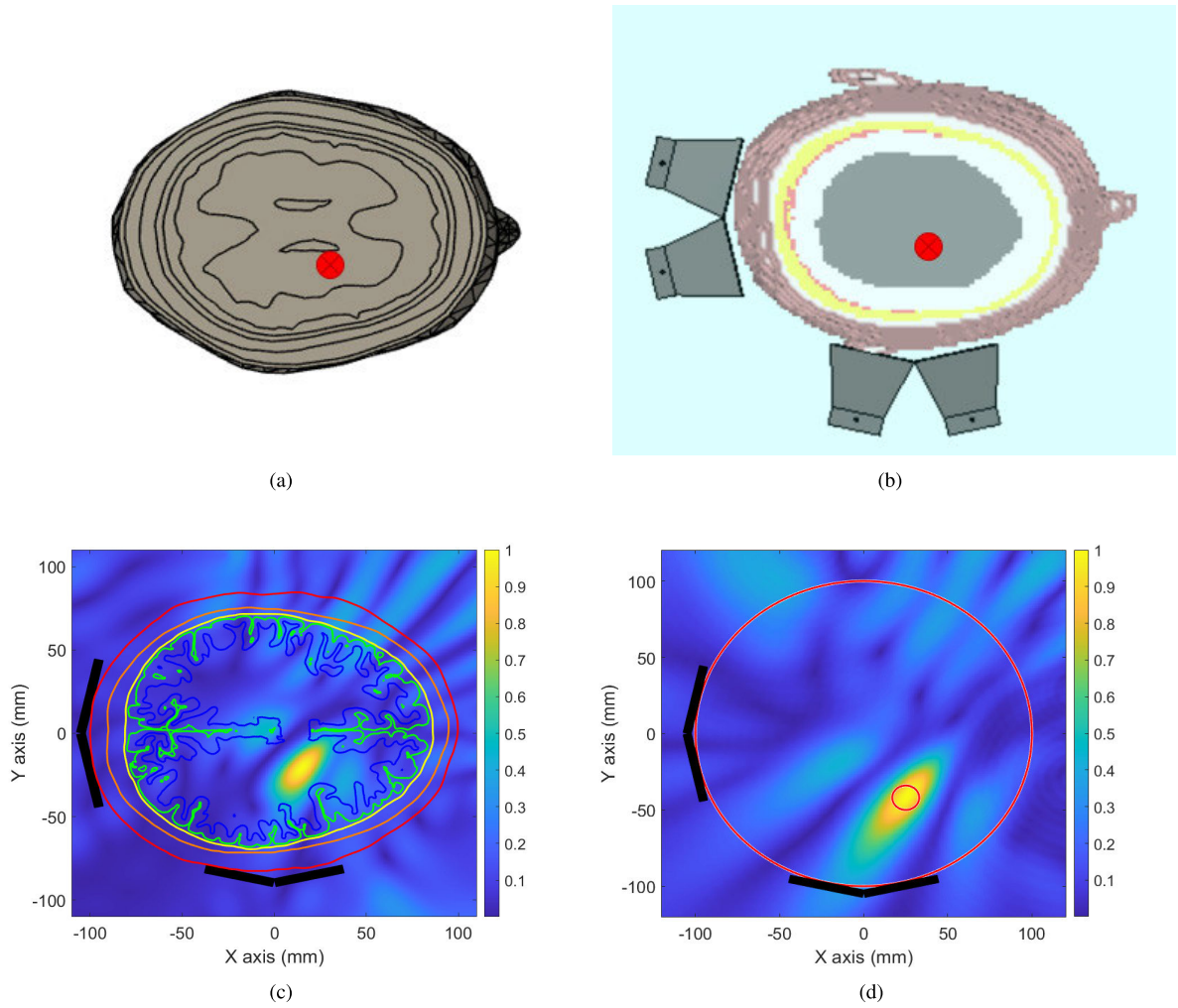

Fig. 8. Reconstructed numerical and experimental microwave images. (a) Basal ganglia is illustrated in a realistic human brain. (b) Numerical simulation of the human head voxel model in CST. (c) Numerical reconstructed image of the human voxel model. (d) Experimentally reconstructed image of the human head phantom.

TABLE II
DIFFERENTIAL MODULATED FIELD OF THE PAM

Analytical differential field	Numerical differential field	Experimental differential field
-92 dB	-94 dB	-95 dB

mentioned in Section II, as in Fig. 8(b). In Fig. 8(c), the numerical microwave image reconstructed for the realistic whole and parts head model are presented in different colors to precisely localize the BT within the brain, which is shown in the right part of the basal ganglia. The experimentally reconstructed image locates precisely the origin of the BT used to generate the brain activity within the zone of interest, as in Fig. 8(d).

In Table II, the comparison of the differential $\Delta S_{21}^{\text{mod}}$ values for the analytical, numerical, and experimental cases is presented. The results show a good agreement and also prove the capability of locating and extracting the low-level signals from a high permittivity medium as the human body. These can help in monitoring functional diseases, as presented in Section IV.

An additional study for the effect of the changes in dielectric properties on the capability of the system to properly locate the origin of the signals was proposed, where a 10% change in permittivity ($\varepsilon_r = 57 \pm 5.7$) results in a 5% location error, which is not significant for the purpose of locating the region where the brain activity is related to the PD.

IV. EXPERIMENTAL VALIDATION OF THE BETA OSCILLATION CHANGES FOR PD

The proposed technique is now explored to study its capability to monitor the changes in the beta frequency band oscillatory character that happens in the BGTC as previously mentioned [14], [30], [31], [32]. To evaluate this part, we propose a beta signal inspired from [14] to see the capability of the system to differentiate between the two signals (healthy and unhealthy) in terms of shape and duration (firing rate). The PD's signal is modeled with a higher value dual-peak and longer duration (lower firing rate) compared to the normal one.

The experimental analysis of differentiating the PD's state from the healthy one is conducted using the same setup, the corresponding functional activity signals were produced in the

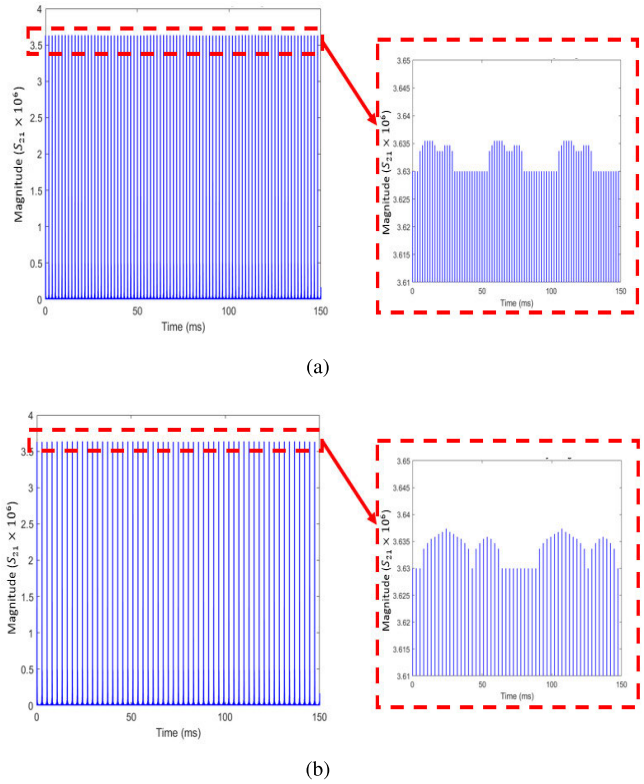

Fig. 9. Measured backscattered PAM signals corresponding to the brain beta band oscillatory activity modeling. (a) Normal state. (b) PD state.

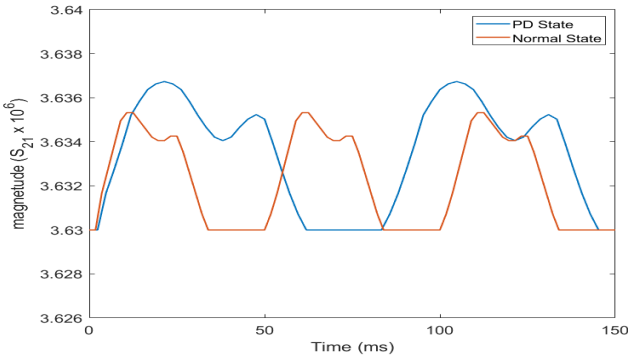

Fig. 10. PD and normal states of the extracted Beta Brain activity model.

BT and the scattering signals were measured for 150 ms. The received PAM signals are presented in Fig. 9(a) for the normal state and in Fig. 9(b) for the PD state.

By analyzing the two signals in Fig. 10, it is observed a frequency difference of 25% (15 Hz for the PD state and 20 Hz for the normal state). This frequency difference corresponds with the values in [52], as mentioned in the introductory part, based on both the firing rate and the shape of the signal [53].

V. Conclusion

This article has presented a novel methodology for monitoring functional neural diseases, and in particular, PD. To model the functional activity within the brain medium, a BT has been designed and tested on generating the AP signal and the proposed technique has proven to be able to extract it from the received PAM signals, as well as locating the origin of those activities using UWB microwave imaging. Based on this technique, we modeled the normal and Parkinson beta oscillation BGTC (which is one of the PD markers), and as a combined result we have been able to extract and locate its origin precisely. This technique will help monitor the brain to detect PD based on the firing rate and brain signal shape.

References

[1] Y. Akazzim, O. El Mrabet, J. Romeu, and L. Jofre-Roca, "Multi-element UWB probe optimization for medical microwave imaging," *Sensors*, vol. 23, no. 1, p. 271, Dec. 2022.

[2] Y. Akazzim, M. Jofre, O. El Mrabet, J. Romeu, and L. Jofre-Roca, "UWB-modulated microwave imaging for human brain functional monitoring," *Sensors*, vol. 23, no. 9, p. 4374, Apr. 2023.

[3] C. Gilmore, A. Zakaria, S. Pistorius, and J. LoVetri, "Microwave imaging of human forearms: Pilot study and image enhancement," *Int. J. Biomed. Imag.*, vol. 2013, pp. 1–17, Jan. 2013.

[4] S. Alani, Z. Zakaria, T. Saeidi, A. Ahmad, M. A. Imran, and Q. H. Abbasi, "Microwave imaging of breast skin utilizing elliptical UWB antenna and reverse problems algorithm," *Micromachines*, vol. 12, no. 6, p. 647, 2021.

[5] M. S. R. Bashri, T. Arslan, W. Zhou, and N. Haridas, "A compact RF switching system for wearable microwave imaging," in *Proc. Loughborough Antennas Propag. Conf. (LAPC)*, Nov. 2016, pp. 1–4.

[6] O. J. Babarinde, M. F. Jamlos, P. J. Soh, D. M. M.-P. Schreurs, and A. Beyer, "Microwave imaging technique for lung tumour detection," in *Proc. German Microw. Conf. (GeMiC)*, Mar. 2016, pp. 100–103.

[7] M. T. Islam, M. Z. Mahmud, M. T. Islam, S. Kibria, and M. Samsuzzaman, "A low cost and portable microwave imaging system for breast tumor detection using UWB directional antenna array," *Sci. Rep.*, vol. 9, no. 1, p. 15491, Oct. 2019.

[8] M. E. Gharbi, M. Martinez-Estrada, R. Fernández-García, and I. Gil, "Determination of salinity and sugar concentration by means of a circular-ring monopole textile antenna-based sensor," *IEEE Sensors J.*, vol. 21, no. 21, pp. 23751–23760, Nov. 2021.

[9] S. R. Mohd Shah et al., "Analysis of thickness variation in biological tissues using microwave sensors for health monitoring applications," *IEEE Access*, vol. 7, pp. 156033–156043, 2019.

[10] A. Cataldo et al., "Portable microwave reflectometry system for skin sensing," *IEEE Trans. Instrum. Meas.*, vol. 71, pp. 1–8, 2022.

[11] X. P. Li et al., "The dynamic dielectric at a brain functional site and an EM wave approach to functional brain imaging," *Sci. Rep.*, vol. 4, no. 1, p. 6893, Nov. 2014.

[12] X. Jiang, Z. Geng, X. Li, L. Peng, B. Kang, and C. Zheng, "Microwave transmission approach for dynamic dielectric detection at brain functional site," in *IEEE MTT-S Int. Microw. Symp. Dig.*, Jun. 2017, pp. 1235–1238.

[13] J.-K. Wang, X. Jiang, L. Peng, X.-M. Li, H.-J. An, and B.-J. Wen, "Detection of neural activity of brain functional site based on microwave scattering principle," *IEEE Access*, vol. 7, pp. 13468–13475, 2019.

[14] Y. Yu et al., "Parkinsonism alters beta burst dynamics across the basal Ganglia–Motor cortical network," *J. Neurosci.*, vol. 41, no. 10, pp. 2274–2286, Mar. 2021.

[15] I. Saied and T. Arslan, "Wideband textile antenna for monitoring neurodegenerative diseases," in *Proc. IEEE 29th Annu. Int. Symp. Pers., Indoor Mobile Radio Commun. (PIMRC)*, Sep. 2018, pp. 356–360.

[16] K. Wirdefeldt, H.-O. Adami, P. Cole, D. Trichopoulos, and J. Mandel, "Epidemiology and etiology of parkinson's disease: A review of the evidence," *Eur. J. Epidemiol.*, vol. 26, pp. 1–58, Jun. 2011.

[17] World Health Organization. *Parkinson Disease*. Accessed: Jul. 5, 2023. [Online]. Available: https://www.who.int/news-room/fact-sheets/detail/parkinson-disease

[18] P. P. Michel, E. C. Hirsch, and S. Hunot, "Understanding dopaminergic cell death pathways in Parkinson disease," *Neuron*, vol. 90, no. 4, pp. 675–691, May 2016.

[19] H. Bernheimer, W. Birkmayer, O. Hornykiewicz, K. Jellinger, and F. Seitelberger, "Brain dopamine and the syndromes of Parkinson and Huntington clinical, morphological and neurochemical correlations," *J. Neurolog. Sci.*, vol. 20, no. 4, pp. 415–455, Dec. 1973.

[20] K. Marek and D. Jennings, "Can we image premotor Parkinson disease?" *Neurology*, vol. 72, no. 7, pp. S21–S26, Feb. 2009. [Online]. Available: https://n.neurology.org/content/72/7Supplement2/S21

[21] R. Prashanth, S. Dutta Roy, P. K. Mandal, and S. Ghosh, "High-accuracy detection of early Parkinson's disease through multimodal features and machine learning," *Int. J. Med. Informat.*, vol. 90, pp. 13–21, Jun. 2016.
[22] K. R. Gandhi and A. Saadabadi, "Levodopa (l-dopa)," in *StatPearls [Internet]*. St. Petersburg, FL, USA: StatPearls Publishing, 2022.
[23] P. S. Larson, "Deep brain stimulation for movement disorders," *Neurotherapeutics*, vol. 11, pp. 465–474, Jul. 2014.
[24] T. M. Herrington, J. J. Cheng, and E. N. Eskandar, "Mechanisms of deep brain stimulation," *J. Neurophysiol.*, vol. 115, no. 1, pp. 19–38, 2016.
[25] M. Delenclos, D. R. Jones, P. J. McLean, and R. J. Uitti, "Biomarkers in parkinson's disease: Advances and strategies," *Parkinsonism Rel. Disorders*, vol. 22, pp. S106–S110, Jan. 2016.
[26] X.-X. Wang et al., "Prodromal markers of Parkinson's disease in patients with essential tremor," *Frontiers Neurol.*, vol. 11, p. 874, Aug. 2020.
[27] E. Hustad and J. O. Aasly, "Clinical and imaging markers of prodromal Parkinson's disease," *Frontiers Neurol.*, vol. 11, p. 395, May 2020.
[28] S. Papapetropoulos, "Preclinical biomarkers of Parkinson disease," *Yearbook Neurol. Neurosurgery*, vol. 2011, pp. 89–90, Jan. 2011.
[29] G. Tomagra et al., "Quantal release of dopamine and action potential firing detected in midbrain neurons by multifunctional diamond-based microarrays," *Frontiers Neurosci.*, vol. 13, p. 288, Apr. 2019.
[30] T. Wichmann, H. Bergamn, and M. DeLong, "Changes in motor behavior and neuronal activity in the internal pallidum induced by subthalamic inactivation in the MPTP model of parkinsonism," *J. Neurophysiol.*, vol. 72, pp. 30–521, Jan. 1994.
[31] A. Nini, A. Feingold, H. Slovin, and H. Bergman, "Neurons in the Globus pallidus do not show correlated activity in the normal monkey, but phase-locked oscillations appear in the MPTP model of parkinsonism," *J. Neurophysiol.*, vol. 74, no. 4, pp. 1800–1805, Oct. 1995.
[32] A. Devergnas, D. Pittard, D. Bliwise, and T. Wichmann, "Relationship between oscillatory activity in the cortico-basal ganglia network and parkinsonism in MPTP-treated monkeys," *Neurobiol. Disease*, vol. 68, pp. 156–166, Aug. 2014.
[33] I. M. Khan et al., "UWB pulse generation and modulation for signal extraction from implantable devices," in *Proc. XX IMEKO World Congr.*, Busan, Republic of Korea, 2012. [Online]. Available: https://www.imeko.org/publications/wc-2012/IMEKO-WC-2012-TC13-O4.pdf
[34] Z. Lin and P. Wei, "Pulse amplitude modulation direct sequence ultra wideband sharing signal for communication and radar systems," in *Proc. 7th Int. Symp. Antennas, Propag. EM Theory*, Oct. 2006, pp. 1–5.
[35] A. Ritzau-Jost et al., "Ultrafast action potentials mediate kilohertz signaling at a central synapse," *Neuron*, vol. 84, no. 1, pp. 152–163, Oct. 2014.
[36] C. Neudorfer et al., "Kilohertz-frequency stimulation of the nervous system: A review of underlying mechanisms," *Brain Stimulation*, vol. 14, no. 3, pp. 513–530, May 2021.
[37] S. Rashid et al., "3-D printed UWB microwave bodyscope for biomedical measurements," *IEEE Antennas Wireless Propag. Lett.*, vol. 18, no. 4, pp. 626–630, Apr. 2019.
[38] (2017). *Recommended Circuit Responsivity Graph*. [Online]. Available: https://www.thorlabs.com/thorproduct.cfm?partnumber=FDS015
[39] B. J. Mohammed and A. M. Abbosh, "Realistic head phantom to test microwave systems for brain imaging," *Microw. Opt. Technol. Lett.*, vol. 56, no. 4, pp. 979–982, Apr. 2014.
[40] J. Sonne, V. Reddy, and M. R. Beato, "Neuroanatomy, substantia nigra," in *StatPearls [Internet]*. St. Petersburg, FL, USA: StatPearls Publishing, 2022.
[41] W. F. Pickard, "Does the resting potential of Chara Braunii have an electrogenic component?" *Can. J. Botany*, vol. 51, no. 4, pp. 715–724, Apr. 1973.
[42] S. H. Wright, "Generation of resting membrane potential," *Adv. Physiol. Educ.*, vol. 28, no. 4, pp. 139–142, Dec. 2004.
[43] G. Franceschetti and I. Pinto, "Cell membrane nonlinear response to an applied electromagnetic field," *IEEE Trans. Microw. Theory Techn.*, vol. MTT-32, no. 7, pp. 653–658, Jul. 1984.
[44] M. Jofre, L. Jofre, and L. Jofre-Roca, "On the wireless microwave sensing of bacterial membrane potential in microfluidic-actuated platforms," *Sensors*, vol. 21, no. 10, p. 3420, May 2021.
[45] (2017). *Fiber-Coupled Led, 455 nm*. [Online]. Available: https://www.thorlabs.com/thorproduct.cfm?partnumber=M455F3
[46] Á. C. Aznar, J. R. Robert, J. M. R. Casals, L. J. Roca, S. B. Boris, and M. F. Bataller, *Antenas*. Barcelona, Spain: Univ. Politèc. de Catalunya, 2004.
[47] P. V. Nikitin, K. V. S. Rao, and R. D. Martinez, "Differential RCS of RFID tag," *Electron. Lett.*, vol. 43, no. 8, p. 431, 2007.
[48] J. C. Bolomey, S. Capdevila, L. Jofre, and J. Romeu, "Electromagnetic modeling of RFID-modulated scattering Mechanism. Application to tag performance evaluation," *Proc. IEEE*, vol. 98, no. 9, pp. 1555–1569, Sep. 2010.
[49] D. M. Lovinger, "Communication networks in the brain: Neurons, receptors, neurotransmitters, and alcohol," *Alcohol Res. Health*, vol. 31, no. 3, p. 196, 2008.
[50] P. Le Floch et al., "Stretchable mesh nanoelectronics for 3D single-cell chronic electrophysiology from developing brain organoids," *Adv. Mater.*, vol. 34, no. 11, Mar. 2022, Art. no. 2106829.
[51] L. Jofre et al., "UWB tomographic radar imaging of penetrable and impenetrable objects," *Proc. IEEE*, vol. 97, no. 2, pp. 451–464, Feb. 2009.
[52] L. Iskhakova et al., "Modulation of dopamine tone induces frequency shifts in cortico-basal ganglia beta oscillations," *Nature Commun.*, vol. 12, no. 1, p. 7026, Dec. 2021.
[53] C. Liu et al., "Closing the loop of DBS using the beta oscillations in cortex," *Cognit. Neurodynamics*, vol. 15, no. 6, pp. 1157–1167, Dec. 2021.

Youness Akazzim received the License degree in electronics and the M.Sc. degree in telecommunication systems engineering from Abdelmalek Essaâdi University, Tetouan, Morocco, in 2016 and 2018, respectively. He is currently pursuing the Ph.D. degree with the Department of Signal Theory and Communications (TSC), in the research group of CommSensLab, Universitat Politècnica de Catalunya (UPC), Barcelona, Spain.

He held a position as a Research Support Technician with the Department of Signal Theory and Communications (TSC), UPC, from 2020 to 2021. In 2017, he joined the Information and Telecommunication Systems Laboratory (LaSIT), Faculty of Sciences, Tetouan, where he has been a Research Assistant. He is currently working on human body parts functionality monitoring using microwave imaging.

Mr. Akazzim has been awarded the Erasmus + Mobility Grant.

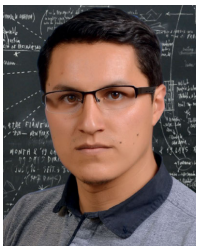

César Palacios Arias (Member, IEEE) received the B.S. degree in telecommunication and electronics engineering from the Private Technical University of Loja UTPL, Loja, Ecuador, in 2013, the M.S. degree in electronics engineering from the University of Calabria, Cosenza, Italy, in 2017. He is currently pursuing the Ph.D. degree with the Department of Signal Theory and Communications (TSC), in the research group of microwave interaction with living organisms, CommSensLab, UPC, Barcelona, Spain.

He has held positions at ALCATEL-LUCENT from 2013 to 2015, Corporación Nacional de Telecomunicaciones-CNT (2015-15), External Researcher at the National University of Chimborazo (2018-), and Research Support Technician at the Department of Signal Theory and Communications (TSC), UPC, (2020 to 2021). He is currently working on microsystems design and manufacturing for communication with living organisms and sensing at X-wave frequencies.

Marc Jofre received the M.Sc. degree in electrical engineering telecommunications, from the Technical University of Catalonia (UPC), BarcelonaTech, Barcelona, Spain, in 2008, jointly with the Technical University of Delft, Delft, The Netherlands, and the Ph.D. degree in photonic sciences from ICFO-The Institute of Photonic Sciences, Castelldefels, Spain, in 2013.

From 2018, he has held different positions at the Technical University of Catalonia (UPC), FPHAG—Fundació Privada Hospital Asil de Granollers, Granollers, Spain, and Max-Planck Institute for Quantum Optics, Garching bei Müchen, Germany. He has published several peer-reviewed articles and granted/transferred patent applications and participated in several funded projects (national and international; competitive and non-competitive). He has extensive experience in innovation, research, project management, intellectual property, and exploitation of quantum technologies for communication and sensing systems, physical characterization of nonlinear materials, biophysical detectors, platforms for the quantification of microorganisms, and health technology.

Otman EL Mrabet (Member, IEEE) received the M.Sc. and Ph.D. degrees from the University of Abdelmalek Essaadi, Tetouan, Morocco, in 2000 and 2004, respectively.

From March to October 2005, he was with the Rennes Institute of Electronics and Telecommunications, Rennes, France, as a Visiting Researcher. From 2007 to 2009, he was a Postdoctoral Researcher, under the AECI Fellowship, with the Department of Electrical and Electronic Engineering, UPNA Pamplona, Spain. Since 2009, he has been an Assistant Professor with the LaSiT Laboratory, in UAE, where he supervises several Ph.D. and M.Sc. theses. He was a Fulbright Scholar at the University of Wisconsin Madison, Madison, Wisconsin, in 2019. His research interests include UWB antenna design, Metamaterials and Metasurfaces, RFID tag antennas, rectennas and wireless power transfer, and modeling active circuits using the finite difference time-domain method (FDTD).

Jordi Romeu (Fellow, IEEE) received the Ingeniero de Telecomunicación and Doctor Ingeniero de Telecomunicación degrees from the Technical University of Catalonia (UPC)-BarcelonaTech, Barcelona, Spain, in 1986 and 1991, respectively.

In 1985, he joined the AntennaLab, Department of Signal Theory and Communications (UPC), where he is currently a Full Professor involved in antenna near-field measurements, electromagnetic scattering and imaging, and system miniaturization for wireless and sensing industrial and bio applications. In 1999, he was a Visiting Scholar at the Antenna Laboratory of the University of California at Los Angeles, Los Angeles, CA, USA, on a NATO Scientific Program Scholarship, and at the University of California at Irvine, Irvine, CA, USA, in 2004. He holds several patents and has published 60 refereed articles in international journals and 80 conference proceedings. He has been involved in the creation of several spin-off companies.

Dr. Romeu was a Grand Winner of the European IT Prize, awarded by the European Commission for his contributions to the development of fractal antennas, in 1998.

Luis Jofre-Roca (Life Fellow, IEEE) received the M.Sc. (Ing.) and Ph.D. (Doctor Eng.) degrees in electronic engineering and telecommunication engineering from the Technical University of Catalonia (UPC), Barcelona, Spain, in 1978 and 1982, respectively.

He has been a Visiting Professor with the École Supérieure d'Electricité Paris from 1981 to 1982, the Georgia Institute of Technology, Atlanta Fulbright Scholar from 1986 to 1987, and the University of California, Irvine, CA, USA, from 2001 to 2002. He was the Director of the Telecommunication Engineering School, UPC, from 1989 to 1994, a Vice President of the UPC from 1994 to 2000, the General Director and Secretary for Catalan Universities and Research from 2011 to 2016, the Director of the Catalan Research Foundation from 2002 to 2004, the Director of the UPC-Telefonica Chair on Information Society Future Trends (2003-), the Principal Investigator of the 2008–2013 Spanish Terahertz Sensing Lab Consolider Project, the Director of the UPC-SEAT Chair on the Future of Automotive, the Research Leader of the 2017–2020 CommSensLab Maria de Maeztu Project, and the Academic Director of the European Consortium for Future Urban Mobility (Carnet). He has authored more than 200 scientific and technical papers, reports, and chapters in specialized volumes. His research interests include antennas, electromagnetic scattering and imaging, system miniaturization for wireless, and sensing for industrial, scientific, and medical applications. His current work focuses on connected reconfigurable autonomous vehicles for urban mobility, massive mimo antennas, and microorganism wireless interaction.

Dr. Jofre-Roca is the Chairperson of the EIT-Urban Mobility European Association.